

Three-level mixing model for nuclear chiral rotation: Role of planar component

Q. B. Chen,^{1,2,*} K. Starosta,^{3,†} and T. Koike^{4,‡}

¹*State Key Laboratory of Nuclear Physics and Technology,
School of Physics, Peking University, Beijing 100871, China*

²*Physik-Department, Technische Universität München, D-85747 Garching, Germany*

³*Department of Chemistry, Simon Fraser University,
8888 University Drive, Burnaby, BC, Canada, V5A 1S6*

⁴*Department of Physics, Tohoku University,
6-3 Aoba Aramaki Aoba Sendai, Japan, 980-8578*

(Dated: March 16, 2022)

Abstract

Three- and two-level mixing models are proposed to understand the doubling of states at the same spin and parity in triaxially-deformed atomic nuclei with odd numbers of protons and neutrons. The Particle-Rotor Model for such nuclei is solved using the newly proposed basis which couples angular momenta of two valence nucleons and the rotating triaxial mean-field into left-handed $|\mathcal{L}\rangle$, right-handed $|\mathcal{R}\rangle$, and planar $|\mathcal{P}\rangle$ configurations. The presence and the impact of the planar component is investigated as a function of the total spin for mass $A \approx 130$ nuclei with the valence $h_{11/2}$ proton particle, valence $h_{11/2}$ neutron hole and the maximum difference between principle axes allowed by the quadrupole deformation of the mean field. It is concluded that at each spin value the higher-energy member of a doublet of states is built on the anti-symmetric combination of $|\mathcal{L}\rangle$ and $|\mathcal{R}\rangle$ and is free of the $|\mathcal{P}\rangle$ component, indicating that it is of pure chiral geometry. For the lower-energy member of the doublet, the contribution of the $|\mathcal{P}\rangle$ component to the eigenfunction first decreases and then increases as a function of the total spin. This trend as well as the energy splitting between the doublet states are both determined by the Hamiltonian matrix elements between the planar ($|\mathcal{P}\rangle$) and non-planar ($|\mathcal{L}\rangle$ and $|\mathcal{R}\rangle$) subspaces of the full Hilbert space.

*Electronic address: qbchen@pku.edu.cn

†Electronic address: starosta@sfu.ca

‡Electronic address: tkoike@lambda.phys.tohoku.ac.jp

A well known example of a two-level quantum system is the parity doublet for a particle in a symmetric Double Square Potential Well (DSPW) [1, 2]. The Hamiltonian for a particle in the DSPW commutes with the parity operator P . Thus eigenstates of the Hamiltonian are eigenstates of the parity. When the potential barrier between the wells forming the DSPW is finite, the positive parity ground state $|+\rangle$ has a partner that is of the negative parity $|-\rangle$ separated by an energy interval related to the height of the potential barrier. When the barrier separating the DSPW wells become infinite the $|+\rangle$ and the $|-\rangle$ partner states become degenerate. In this case linear combinations of the $|\pm\rangle$ eigenstates can be formed,

$$|\mathcal{L}/\mathcal{R}\rangle = 1/\sqrt{2}(|+\rangle \mp |-\rangle), \quad (1)$$

with the $|\mathcal{L}/\mathcal{R}\rangle$ states being the eigenstates of the Hamiltonian but not the parity operator. The $|\mathcal{L}/\mathcal{R}\rangle$ states represent in this particular case the lowest-energy solution in the infinite potential well on the right or the left of the DSPW for which $P|\mathcal{L}\rangle = |\mathcal{R}\rangle$ or vice versa. In the case of the infinite barrier the $|\pm\rangle$ as well as the $|\mathcal{L}/\mathcal{R}\rangle$ states describe system equally well. Thus, there is a freedom of choice in selecting the former set of well defined parity, or the latter set for which the parity is not defined, but the interpretation of the wave function of a particle confined to either the left or the right well is intuitive.

For the last two decades, a novel two-level quantum mechanical system involving three axial vectors of angular momenta has been under intensive scrutiny in relation to coupling of collective and single particle motions in rotating nuclei [3]. For an odd-odd rotating nucleus with a triaxial shape (a shape of a kiwi fruit) and valence proton/neutron in high- j particle/hole orbitals, the total angular momentum \vec{I} may lie outside of the three principal planes. Consequently, the three components of the total angular momentum along the principal axes can be oriented in either left- or right-handed systems, thus defining chirality. The left- and the right-handed systems are transformed into each other by the chiral operator which combines spatial rotation by 180° around the intermediate axis with the time reversal, $\mathcal{R}_2(\pi)\mathcal{T}$ [4]. The formation of chiral systems takes place in the reference frame which is defined by the principle axes of the deformed nuclear mean field. This is a rotating, thus non-inertial reference frame. In the stationary, thus inertial, laboratory reference frame, the wave functions are linear combinations which include with equal probability the left-handed and right-handed components. This leads to the doubling of states in the laboratory frame referred to as “restoration of chiral symmetry”. Consequently, the transformation to the

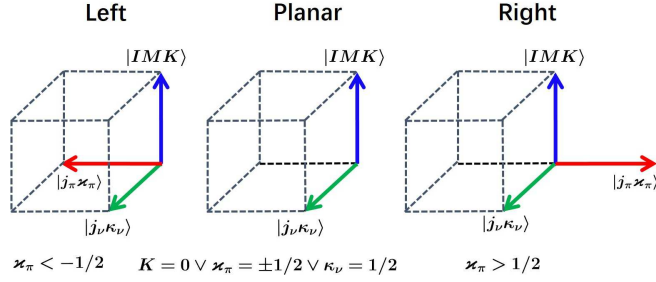


FIG. 1: (Colour online) Cartoons of angular momentum coupling for the left-handed, planar, and right-handed bases.

laboratory frame gives rise to a pair of nearly degenerate $\Delta I = 1$ bands with the same parity, often referred to as chiral doublet bands [3].

The purpose of this Rapid Communication is to analyze models for the doubling of states related to chiral coupling of angular momenta vectors drawing analogies to the DSPW model of parity doublets. The models presented here, while simplified, capture the essential physics of nuclear chiral rotation. In particular, the mechanism leading to energy degeneracy and the role of non-chiral (planar) component are illustrated. On the other hand, while the behaviour of the chiral system bears strong analogies to the DSPW, there is one prominent difference should be emphasized. In the DSPW model the potential barrier is static, while in the case of nuclear chirality the barrier height for systems of opposite chirality depends on the total angular momentum of the rotating nucleus, although it is static at a given I .

Among various nuclear models, the Particle Rotor Model (PRM) has been widely used to describe the chiral doublet bands achieving major successes [3, 5–12]. The model, with the particular Hamiltonian for coupling of a proton particle and a neutron hole considered here

$$H = H_R + H_\pi - H_\nu, \quad (2)$$

describes in the laboratory reference frame a system consisting of collective rotation of a triaxially deformed body

$$H_R = \sum_{i=1}^3 \frac{R_i^2}{2\mathcal{J}_i} \quad (3)$$

and single-particle motion of valence nucleons in the body-fixed quadrupole-deformed mean

field potential

$$H_{\pi/\nu} = -\kappa(r)\beta [\cos \gamma Y_{2,0}(\theta, \phi) + \frac{1}{\sqrt{2}} \sin \gamma (Y_{2,2}(\theta, \phi) + Y_{2,-2}(\theta, \phi))] \quad (4)$$

with β and γ representing standard quadrupole-deformation parameters and $\kappa(r)$ denoting radial dependence. The total angular momentum of the system is

$$\vec{I} = \vec{R} + \vec{j}_\pi + \vec{j}_\nu. \quad (5)$$

So far, chiral geometry of angular momentum coupling has been extracted from expectation values of orientation operators, rather than being a starting point at the outset of solving the PRM. Very recently Ref. [13] proposed to solve the PRM in the Hilbert space that contains subspaces of left-handed, right-handed, and planar states of angular momentum coupling. The basis states are defined by Eq. 95 of Ref. [13]

$$\begin{aligned} |IMK j_\pi \varkappa_\pi j_\nu \kappa_\nu\rangle &= \quad (6) \\ &= \frac{1}{2} \sqrt{\frac{2I+1}{8\pi^2}} (D_{MK}^I(\omega) |j_\pi \varkappa_\pi\rangle |j_\nu \kappa_\nu\rangle \\ &+ (-1)^{I-j_\pi-\kappa_\nu} D_{M\bar{K}}^I(\omega) |j_\pi \bar{\varkappa}_\pi\rangle |j_\nu \kappa_\nu\rangle \\ &+ (-1)^{I+K+j_\nu-\varkappa_\pi+\kappa_\nu} D_{M\bar{K}}^I(\omega) |j_\pi \varkappa_\pi\rangle |j_\nu \bar{\kappa}_\nu\rangle \\ &+ (-1)^{K+j_\pi+j_\nu-\varkappa_\pi} D_{MK}^I(\omega) |j_\pi \bar{\varkappa}_\pi\rangle |j_\nu \bar{\kappa}_\nu\rangle), \\ \bar{K} &= -K, \quad \bar{\varkappa}_\pi = -\varkappa_\pi, \quad \bar{\kappa}_\nu = -\kappa_\nu, \\ &\text{for } K > 0, \quad \varkappa_\pi \in [-j_\pi, j_\pi], \quad \kappa_\nu \in [1/2, j_\nu], \\ &\text{for } K = 0, \quad \varkappa_\pi \in [1/2, j_\pi], \quad \kappa_\nu \in [1/2, j_\nu]. \end{aligned}$$

with K , \varkappa_π and κ_ν representing the projection of I , j_π and j_ν on the intermediate-, short-, and the long-axis of the triaxial mean field, respectively. The restrictions on ranges of quantum numbers K , \varkappa_π and κ_ν are set to span the full Hilbert space while eliminating states which differ by a phase only. The choice of $K \geq 0$ and $\kappa_\nu \geq 1/2$ is a convention adopted here following Ref. [13]. For the above basis states, the handedness is an explicit property defined by the sign of \varkappa_π as shown in Fig. 1 and is defined prior to diagonalization of the Hamiltonian rather than extracted feature as in models with non-chiral bases.

In details, the left-handed \mathcal{L} , the right-handed \mathcal{R} , and the planar \mathcal{P} subspaces are defined as

$$\mathcal{L} = \{K > 0 \wedge \varkappa_\pi < -1/2 \wedge \kappa_\nu > 1/2\},$$

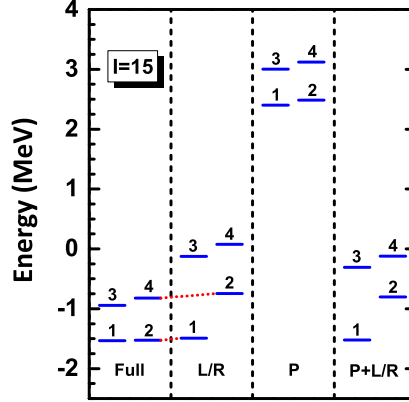


FIG. 2: (Colour online) Energies from diagonalization of the PRM Hamiltonian at spin $I = 15$ in combination of subspaces of Eq. 7. The four combinations are: full basis (Full); left/right block (\mathcal{L}/\mathcal{R}), planar block (\mathcal{P}), and planar plus left/right blocks ($\mathcal{P} + \mathcal{L}/\mathcal{R}$). The four lowest energy states labelled as 1-4, respectively, are shown in each spectrum.

$$\begin{aligned}\mathcal{R} &= \{K > 0 \wedge \varkappa_\pi > 1/2 \wedge \kappa_\nu > 1/2\}, \\ \mathcal{P} &= \{K = 0 \vee \varkappa_\pi = \pm 1/2 \vee \kappa_\nu = 1/2\}.\end{aligned}\quad (7)$$

The sum of the three subspaces is referred to as the “Full” Hilbert space. Under the action of the operator $\mathcal{R}_2(\pi)\mathcal{T}$ the \mathcal{L} and \mathcal{R} subspaces are transformed to each other, while the \mathcal{P} subspace is invariant. The leading-order Coriolis matrix elements are contained within each subspace leading to nearly block-diagonal structure of the Hamiltonian matrix. Current work explores impact of the coupling between the planar and the chiral subspaces.

Figure 2 presents results of block diagonalization of the PRM Hamiltonian in the combinations of subspaces of Eq. 7 in comparison to the diagonalization in the Full basis. The results are obtained for a symmetric particle-hole configuration $\pi(1h_{11/2})^1 \otimes \nu(1h_{11/2})^{-1}$ corresponding to the $A \approx 130$ mass region and the deformation parameters $\beta = 0.18$ and $\gamma = 90^\circ$. The coupling constant for the nuclear mean field potential defined by Eq. 13 of Ref. [13] has been assumed as $0.24 \text{ MeV}/\hbar^2$ while the irrotational flow moments of inertia $\mathcal{J}_3 = 4\mathcal{J}_1 = 4\mathcal{J}_2 = \mathcal{J}_0$ are adopted with $\mathcal{J}_0 = 30 \text{ } \hbar^2/\text{MeV}$. These parameters result in formation of the chiral doublet bands and yield degeneracy of states at the total spin value of $I = 15^+$ as reported previously in Refs. [13] and [3]. As seen in Fig. 2, the energies resulting from the diagonalization in the Full space are the lowest, which is expected for the complete basis. The nearly degenerate levels 1 and 2 as well as levels 3 and 4 are attributed

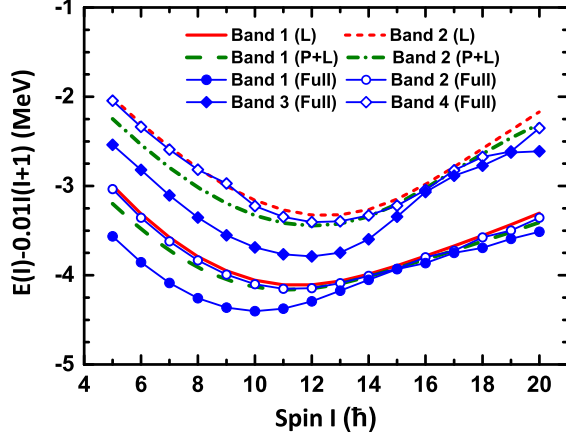


FIG. 3: (Colour online) For the lowest two pairs of chiral doublet (bands 1-2 and 3-4) a comparison of diagonalization of the PRM Hamiltonian in the Full, \mathcal{L} , and $\mathcal{P} + \mathcal{L}$ subspaces.

to the exactly degenerate solutions in the \mathcal{L} and \mathcal{R} subspaces. The lowest-energy solutions in the diagonalization in the \mathcal{P} subspace are separated from the lowest-energy solutions in the \mathcal{L}/\mathcal{R} subspaces by a sizable ≈ 5 MeV energy gap. Consequently, the lowest-energy state from block diagonalization in the $\mathcal{P} + \mathcal{L}/\mathcal{R}$ space is nearly at the same energy as levels 1 and 2 from the diagonalization in the Full space, in good analogy to the DSPW model.

In Fig. 2, it is further observed that the levels 1 and 2 from diagonalization in the \mathcal{L}/\mathcal{R} subspace are nearly at the same energy as levels 2 and 4 from diagonalization in the Full space, respectively. The energy difference between the states of the same spins in the doublet band are less than 200 keV in a large spin window around the most degenerate levels at spin 15. Hence, the 5 MeV separation energy between the lowest-energy solutions in the \mathcal{L}/\mathcal{R} and \mathcal{P} subspaces indicated by Fig. 2 is indeed a sizable gap compared with the energy of separation of the doublet band members. Since calculations in Fig. 2 are for spin $I = 15$, a question arises if this observation is representative for the whole spin region. To investigate further, the corresponding lowest energy spectra as a function of spin are shown in Fig. 3 with bands labelled following the convention used in Fig. 2. It can be observed in Fig. 3 that bands 1 and 2 from diagonalization in the \mathcal{L}/\mathcal{R} subspace can very well reproduce bands 2 and 4 from diagonalization in the Full space, respectively, and that bands 1 and 2 from diagonalization in the $\mathcal{P} + \mathcal{L}/\mathcal{R}$ subspace are lower in energy than those from the diagonalization in the \mathcal{L}/\mathcal{R} subspace.

To understand the above observation we propose a three energy level model (3-ELM) for the Full diagonalization based on a simplification which assumes that the $|\mathcal{L}\rangle$, $|\mathcal{R}\rangle$, and $|\mathcal{P}\rangle$ subspaces consist of a single basis state each. Note that for $\gamma = 90^\circ$ $\langle\mathcal{L}|H|\mathcal{R}\rangle = \langle\mathcal{R}|H|\mathcal{L}\rangle = 0$ and consequently the Hamiltonian matrix takes the form

$$H = \begin{pmatrix} \langle\mathcal{L}|H|\mathcal{L}\rangle & \langle\mathcal{L}|H|\mathcal{R}\rangle & \langle\mathcal{L}|H|\mathcal{P}\rangle \\ \langle\mathcal{R}|H|\mathcal{L}\rangle & \langle\mathcal{R}|H|\mathcal{R}\rangle & \langle\mathcal{R}|H|\mathcal{P}\rangle \\ \langle\mathcal{P}|H|\mathcal{L}\rangle & \langle\mathcal{P}|H|\mathcal{R}\rangle & \langle\mathcal{P}|H|\mathcal{P}\rangle \end{pmatrix} = \begin{pmatrix} \mathcal{A} & 0 & \mathcal{C} \\ 0 & \mathcal{A} & \mathcal{C} \\ \mathcal{C}^* & \mathcal{C}^* & \mathcal{B} \end{pmatrix}. \quad (8)$$

Results presented in Figs. 2 and 3 indicate $\mathcal{B} \gg \mathcal{A}$. The energy-ordered eigenvalues of Eq. 8

$$\begin{aligned} \lambda_1 &= \frac{1}{2} \left[(\mathcal{B} + \mathcal{A}) - \sqrt{(\mathcal{B} - \mathcal{A})^2 + 8\mathcal{C}^2} \right], \\ \lambda_2 &= \mathcal{A}, \\ \lambda_3 &= \frac{1}{2} \left[(\mathcal{B} + \mathcal{A}) + \sqrt{(\mathcal{B} - \mathcal{A})^2 + 8\mathcal{C}^2} \right], \end{aligned} \quad (9)$$

correspond to three eigenstates

$$\begin{aligned} \psi_1 &= \frac{1}{\sqrt{N_1}} \begin{pmatrix} \frac{1}{4} \left[(\mathcal{A} - \mathcal{B}) - \sqrt{(\mathcal{A} - \mathcal{B})^2 + 8\mathcal{C}^2} \right] \\ \frac{1}{4} \left[(\mathcal{A} - \mathcal{B}) - \sqrt{(\mathcal{A} - \mathcal{B})^2 + 8\mathcal{C}^2} \right] \\ \mathcal{C}^* \end{pmatrix}, \\ \psi_2 &= \frac{1}{\sqrt{2}} \begin{pmatrix} 1 \\ -1 \\ 0 \end{pmatrix}, \\ \psi_3 &= \frac{1}{\sqrt{N_3}} \begin{pmatrix} \frac{1}{4} \left[(\mathcal{A} - \mathcal{B}) + \sqrt{(\mathcal{A} - \mathcal{B})^2 + 8\mathcal{C}^2} \right] \\ \frac{1}{4} \left[(\mathcal{A} - \mathcal{B}) + \sqrt{(\mathcal{A} - \mathcal{B})^2 + 8\mathcal{C}^2} \right] \\ \mathcal{C}^* \end{pmatrix}, \end{aligned} \quad (10)$$

with N_i denoting normalization of ψ_i for $i = 1$ and 3 .

Based on the above results, it is interesting to note that $\lambda_2 = \mathcal{A} = \langle\mathcal{L}|H|\mathcal{L}\rangle = \langle\mathcal{R}|H|\mathcal{R}\rangle$. This explains why the energy spectra obtained by diagonalization in the \mathcal{L}/\mathcal{R} subspace

reproduce part of the results of diagonalization in the Full space, as shown in Figs. 2 and 3. Also, note that in the ψ_2 eigenfunction $|\mathcal{L}\rangle$ and $|\mathcal{R}\rangle$ contributions mix equally with the opposite phase forming an anti-symmetric combination which contains only pure chiral components and does not include any $|\mathcal{P}\rangle$ component. Next, consider eigenstates ψ_1 and ψ_3 . For these states $|\mathcal{L}\rangle$ and $|\mathcal{R}\rangle$ components contribute equally with the same phase and also the planar component is admixed; this makes them distinctively different from the ψ_2 state. Due to the fact that $\mathcal{B} \gg \mathcal{A}$ the $|\mathcal{P}\rangle$ component in the ψ_1 state is much smaller than $|\mathcal{L}\rangle$ and $|\mathcal{R}\rangle$ components. Correspondingly, the ψ_3 state is at high energy (≈ 5 MeV higher than ψ_1) and with dominating $|\mathcal{P}\rangle$ component. High excitation energy is the most likely reason why this state has not yet been observed.

Similarly, we can also construct a two energy level model (2-ELM) for $\mathcal{P} + \mathcal{L}$ block diagonalization as

$$H = \begin{pmatrix} \langle \mathcal{L} | H | \mathcal{L} \rangle & \langle \mathcal{L} | H | \mathcal{P} \rangle \\ \langle \mathcal{P} | H | \mathcal{L} \rangle & \langle \mathcal{P} | H | \mathcal{P} \rangle \end{pmatrix} = \begin{pmatrix} \mathcal{A} & \mathcal{C} \\ \mathcal{C}^* & \mathcal{B} \end{pmatrix}. \quad (11)$$

The energy-ordered eigenvalues are

$$\Lambda_{\mp} = \frac{1}{2} \left[(\mathcal{B} + \mathcal{A}) \mp \sqrt{(\mathcal{B} - \mathcal{A})^2 + 4\mathcal{C}^2} \right]. \quad (12)$$

Note that $\mathcal{B} \gg \mathcal{A}$ implies $\lambda_1 < \Lambda_- < \lambda_2$. For that reason block diagonalization in the $\mathcal{P} + \mathcal{L}$ subspace yields energies lower than block diagonalization in the \mathcal{L}/\mathcal{R} or \mathcal{P} subspaces but higher than the diagonalization in the Full space, as indeed illustrated in Figs. 2 and 3.

Based on the conclusions drawn above, the values of effective interaction \mathcal{C} is extracted. In the 3-ELM according to Eq. 9

$$\mathcal{C}_{\text{Full}} = \sqrt{\frac{1}{2}(\mathcal{A} - \lambda_1)(\mathcal{B} - \lambda_1)}, \quad (13)$$

where \mathcal{A} , \mathcal{B} , and λ_1 are taken as the lowest solution from diagonalization in the \mathcal{L} , \mathcal{P} , and Full subspaces, respectively. Similarly, one can extract \mathcal{C} from the 2-ELM using Λ_- of Eq. 12. The results are presented in Fig. 4 as a function of spin. The magnitude of the interaction is $\mathcal{C} \approx 1$ MeV through the whole spin region.

According to the 3-ELM if $\mathcal{C} = 0$, then $\lambda_2 = \lambda_1$ and ψ_1 and ψ_2 are strictly degenerate. In this case the ψ_1 and ψ_2 wave functions contain only $|\mathcal{L}\rangle$ and $|\mathcal{R}\rangle$ chiral components mixed with the same or the opposite phase but without any $|\mathcal{P}\rangle$ contribution. With the increase of \mathcal{C} the degeneracy is gradually broken. Consequently, the magnitude of \mathcal{C} determines the

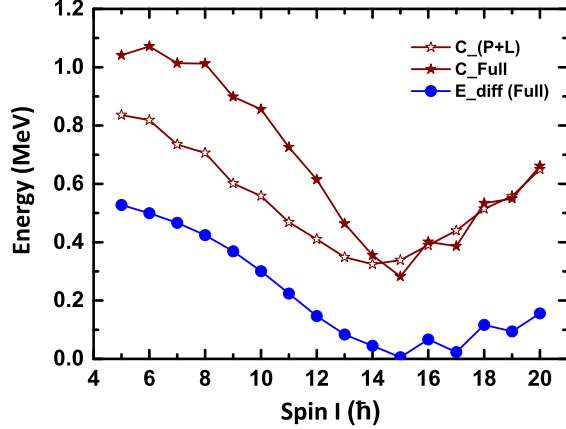


FIG. 4: (Colour online) The effective interactions $\mathcal{C} = \langle \mathcal{L} | H | \mathcal{P} \rangle$ extracted from the three energy level model (3-ELM) ($\mathcal{C}_{\text{Full}}$) and the two energy level model (2-ELM) ($\mathcal{C}_{\mathcal{P}+\mathcal{L}}$) as a function of spin I , in comparison with the energy difference between the lowest pair of chiral doublet bands in the full diagonalization.

energy splitting between the chiral doublet bands. Figure 4 presents the energy differences between the lowest pair of chiral doublet bands as a function of spin in comparison with the magnitude of \mathcal{C} extracted using Eq. 13. The magnitude of \mathcal{C} first decreases and then increases as a function of spin. The turning point is at $I \approx 15$ and $I \approx 14$ for $\mathcal{C}_{\text{Full}}$ and $\mathcal{C}_{\mathcal{P}+\mathcal{L}}$, respectively. The change of the magnitude of \mathcal{C} correlates very well with the variation of energy difference between the members of the lowest-energy doublet band. Particularly, for $\mathcal{C}_{\text{Full}}$ an odd-even staggering behaviour is extracted at the spin region $I \geq 15$ which is also observed for the energy difference. In conclusion, the behaviour of the energy difference between the doublet bands is determined by the interaction matrix elements between the planar and non planar subspaces of the full Hilbert space. To emphasize the analogy to the DSPW model, we postulate that $1/\mathcal{C}$ corresponds to barrier height between the left- and the right-handed potential wells. If \mathcal{C} approaches zero the barrier height approaches infinity and chiral doublets become degenerate. The increase of \mathcal{C} corresponds to the decrease of potential barrier and thus leads to the interaction between $|\mathcal{L}/\mathcal{R}\rangle$ and $|\mathcal{P}\rangle$ subspaces which lifts the degeneracy between doublet states.

According to the 3-ELM states, band 2 do not contain the \mathcal{P} component, while the contribution of \mathcal{P} component to states in band 1 is small relative to \mathcal{L} and \mathcal{R} components. This is illustrated in Fig. 5 showing a comparison of squared amplitudes of \mathcal{L}/\mathcal{R} and \mathcal{P}

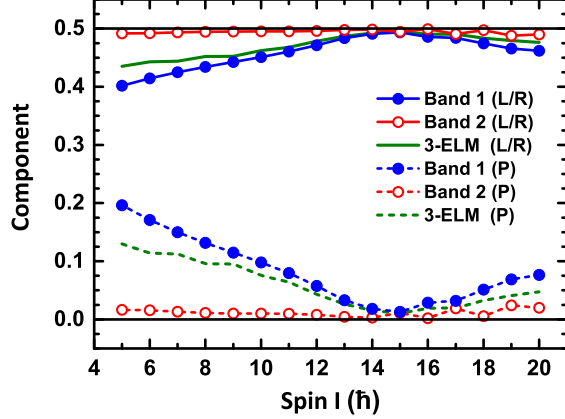


FIG. 5: (Colour online) For the lowest energy chiral doublet band, a comparison of squared amplitudes of \mathcal{L}/\mathcal{R} and \mathcal{P} components as a function of spin from the 3-ELM and from full diagonalization.

components as a function of spin for states in bands 1 and 2 from the 3-ELM and from full diagonalization. It is observed that full diagonalization for band 2 leads to nearly vanishing contribution of \mathcal{P} and $\approx 50\%$ contribution of \mathcal{L} and \mathcal{R} components in full consistency with 3-ELM predictions. Consequently, band 2 can be considered as of pure chiral geometry. For band 1 the contribution of planar components shows a dependence on spin similar to that for \mathcal{C} in Fig. 4, decreasing up to $I = 15$ and then increasing as a function of increasing spin. Correspondingly, the $|\mathcal{L}\rangle$ or $|\mathcal{R}\rangle$ components increase and then decrease. At $I = 15$ bands 1 and 2 are separated by the smallest energy interval presenting the best case of static chirality, nearly without the tunnelling between the $|\mathcal{L}\rangle$ and $|\mathcal{R}\rangle$ components. These analyses strongly suggest that chiral geometry is rather robust as manifested in the band 2, while the degeneracy of states with the same spin and parity occurs only in a limited spin range. Again, properties of band 1 resulting from full diagonalization agree well with predictions of the 3-ELM, which further indicates that 3-ELM provides useful tools for understanding results of exact diagonalization of the PRM.

In summary, three- and two-level mixing models are proposed to understand the degeneracy of the chiral doublet bands. It is identified that the higher-energy member of a chiral doublet band is formed by anti-symmetric combination of chiral components; it is of pure chiral geometry without any planar components. For the lowest-energy band member planar components show first a decreasing and then increasing trend with spin. This trend as well as the magnitude of the energy splitting between both members are determined by matrix

elements of the Hamiltonian between the planar and nonplanar subspaces of the full PRM Hilbert space.

The different planar components in the chiral doublet bands would be used to interpret other possible different properties in the chiral doublets, which provide impetus to reexamine the fingerprints of the chiral doublets, such as electromagnetic transitions and angular momentum geometries.

Acknowledgments

Q.B.C wants to thank F. Q. Chen, J. Meng, and S. Q. Zhang for fruitful discussions. Financial support for this work was provided in parts by the Major State 973 Program of China (Grant No. 2013CB834400), the National Natural Science Foundation of China (NSFC) under Grants No. 11335002, No. 11375015, No. 11461141002, and No. 11621131001, the China Postdoctoral Science Foundation under Grants No. 2015M580007 and No. 2016T90007, the Deutsche Forschungsgemeinschaft (DFG) and NSFC through funds provided to the Sino-German CRC 110 “Symmetries and the Emergence of Structure in QCD”, and the Natural Sciences and Engineering Research Council of Canada.

-
- [1] J. J. Sakurai, *Modern Quantum Mechanics* (Addison-Wesley Publishing Company, 1994).
 - [2] R. P. Feynman, *The Feynman lectures on physics III: quantum mechanics* (New York : Addison-Wesley, 1965).
 - [3] S. Frauendorf and J. Meng, Nucl. Phys. A **617**, 131 (1997).
 - [4] S. Frauendorf, Rev. Mod. Phys. **73**, 463 (2001).
 - [5] K. Starosta, T. Koike, C. J. Chiara, D. B. Fossan, and D. R. LaFosse, Nucl. Phys. A **682**, 375c (2001).
 - [6] J. Peng, J. Meng, and S. Q. Zhang, Phys. Rev. C **68**, 044324 (2003).
 - [7] T. Koike, K. Starosta, and I. Hamamoto, Phys. Rev. Lett. **93**, 172502 (2004).
 - [8] S. Q. Zhang, B. Qi, S. Y. Wang, and J. Meng, Phys. Rev. C **75**, 044307 (2007).
 - [9] B. Qi, S. Q. Zhang, J. Meng, S. Y. Wang, and S. Frauendorf, Phys. Lett. B **675**, 175 (2009).
 - [10] E. A. Lawrie and O. Shirinda, Phys. Lett. B **689**, 66 (2010).

- [11] S. G. Rohozinski, L. Prochniak, K. Starosta, and C. Droste, *Eur. Phys. J. A* **47**, 90 (2011).
- [12] O. Shirinda and E. A. Lawrie, *Eur. Phys. J. A* **48**, 118 (2012).
- [13] K. Starosta and T. Koike, *Phys. Scr.* **92**, 093002 (2017).